14

The Use of The Principal Components of Transverse Wavefront Aberrations in Model-Based Control Algorithms for Adaptive Optics

© D.A. Yagnyatinskiy[1], A.P. Kuznetsov[2]

[1] V.E. Zuev Institute of Atmospheric Optics, Siberian Branch, Russian Academy of Sciences, Tomsk, Russia
[2] National Research Nuclear University MEPhI, Moscow, Russia

e-mail: lambsky@yandex.ru

Received September 02, 2025
Revised November 16, 2025
Accepted January 23, 2026

For model-based adaptive optics control algorithms based on measuring the rms focal spot radius with an intensity sensor, we propose to use the principal components of transverse wavefront aberrations as control modes. These components are the Karhunen-Loéve-Lukosz functions corresponding to the given phase-distortion statistics. The approach is demonstrated for the Kolmogorov turbulence model of the optical medium. By means of numerical simulation, we compared the performance of algorithms for two bases of control modes: Lukosz polynomials and Karhunen-Loéve-Lukosz functions. The use of Karhunen-Loéve-Lukosz modes instead of Lukosz modes was shown to statistically reduce the wavefront RMS error and improve the focusing of the laser beam. It was found that Karhunen-Loéve-Lukosz modes are also preferable to Lukosz modes in that they allow for a more precise measurement of mode coefficients by aperture probing. The simulations were performed for an ideal corrector and for the optimized models of a stacked-array piezoelectric deformable mirror.

Keywords: adaptive optics, control algorithms, rms focal spot radius, aberrations, Kolmogorov turbulence model, Lukosz polynomials, Karhunen-Loéve-Lukosz functions, deformable mirror.

DOI: 10.61011/EOS.2026.02.63472.8529-25

Introduction

Control algorithms for adaptive optics systems (AOS) that use aperture probing [1,2] are usually divided [3] into two main categories: blind search algorithms and deterministic search algorithms, which rely on physical properties of the optical system model. (In the authors' opinion, a third category neural-network-based algorithms can now be identified, but we shall not discuss it here.) Blind search („model-free") algorithms, which do not account for the properties of the AOS model, appeared first. Over time, a large number of their varieties were developed, in particular [4–11]. An important alternative to these algorithms are model-based algorithms that use the rms focal spot radius measured on the intensity sensor as the target function (optimization criterion) [12–19]. By theoretical design, their main advantage is an extremely low number of test perturbations required to measure the wavefront shape. These algorithms retrieve unknown aberration coefficients in a specified mode basis. Let us remark that, since the most of processing time in the AOS is spent on signaling the corrector and its subsequent reproduction of the target shape, we characterize the algorithms mainly by the number of iterations that involve the physical actuation of the deformable mirror, rather than by the number of measurements on the intensity sensor, as is usual in papers on this subject [12–17,19,20]. Numerical simulation and experiments show [20,16] that model-based algorithms may be more efficient than blind search algorithms in correcting the wavefront of optical radiation.

Fig. 1 shows a typical scheme of AOS operation using aperture probing in closed-loop mode. The distorted wavefront of the incoming radiation is incident on the aperture of the deformable mirror. The radiation is then split into two beams with the beam splitter. One of the beams remains in the control circuit. Having passed lens 1, it arrives at the photodetector, which registers the intensity distribution in the focal spot. Test perturbations are applied to the deformable mirror as aberration base modes. Then control signals for the next iteration are generated to decrease the rms spot radius. As a result, after several iterations the shape of the mirror becomes close to the shape of the incoming wavefront. The other beam exits the splitter and the control circuit with a corrected wavefront. It may then be directed to the focusing lens 2.

In the model-based algorithms considered, special control modes that have mutually orthogonal gradients at the given aperture are used to apply test perturbations. This ensures independent impacts of the base modes on the rms focal spot radius and allows them to be corrected independently with high precision, eliminating the „$2N\pi$-problem of local extrema" [21], which is present in many existing aperture probing algorithms (most frequently this problem occurs when the Strehl ratio is used as a criterion). Model-based algorithms implement modal control. Since modes as factors impact the optimization criterion independently, the problem of local extrema does not arise.

Among wavefront representation modes that have orthogonal gradients, Lukosz polynomials (L) [22,23] are most commonly used. In addition to the above property, they are

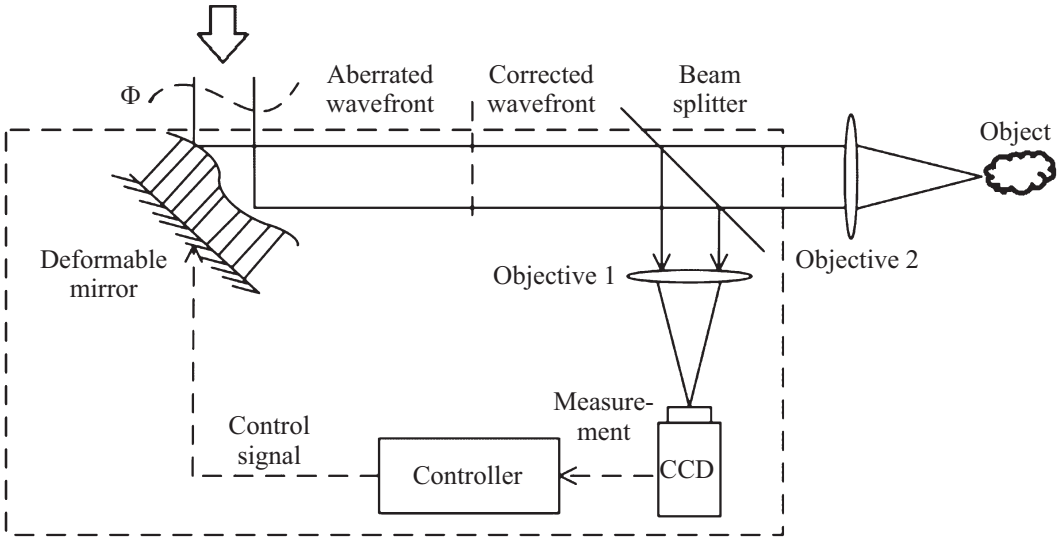

Figure 1. A typical AOS using a model-based algorithm.

also balanced in terms of minimizing the variance of their transverse (ray) aberrations [24]. In [25], these polynomials were transformed into another basis set; the Karhunen–Loéve–Lukosz functions (*LKL*), which are the principal components of geometric transverse aberrations for a set of wavefronts with a given statistics of phase distortions. The resulting new functions retain the key property of the mutual orthogonality of their gradients and can therefore be used in model-based algorithms in the same way as Lukosz polynomials. Unlike [25], here, for modal correction, we compare only two mode bases — *L* and *LKL*, since the other widely used bases do not satisfy the condition of gradient orthogonality.

The distinctive feature of *LKL* modes, as specified in [25], is that subtracting them from the initial wavefronts statistically minimizes the rms spot radius, i.e. the optimization criterion is minimized in the model-based algorithms that we consider. The purpose of this paper is to demonstrate the advantage of Karhunen-Loéve-Lukosz functions over Lukosz polynomials in these algorithms. As in [25], we consider the statistics of phase distortions corresponding to the Kolmogorov spectrum of atmospheric turbulence [26,27] (for brevity, we will refer to the corresponding wavefronts and turbulence as „Kolmogorov“ [26,27], as is common in informal speech and the literature [27]). This wavefront distortion model closely approximates real atmospheric conditions in many practical cases, although it has its limitations [26,27].

1. Mathematical description of model-based algorithms that minimize rms spot radius

Let there be a non-apodized laser beam with wavelength λ and a certain wavefront. We expand this wavefront (in phase units) in Lukosz polynomials $\{L_j\}$ with aberration coefficients $\{b_j\}$:

$$\Phi = \sum_{j=1}^{\infty} b_j L_j. \tag{1}$$

It is known that for the basis modes $\{L_j\}$ the following property holds [15]:

$$\iint\limits_{O_1} \nabla L_j \nabla L_{j'} d\sigma = \pi \delta_{jj'}, \tag{2}$$

where O_1 is a circle of unit radius (the transverse coordinates are normalized accordingly), ∇ is the gradient operator, and δ is the Kronecker delta. Then, for a circular aperture in the geometric optics approximation, the rms spot radius R expressed in terms of the Lukosz aberration coefficients $\{b_j\}$ is given by [28]:

$$R^2 = \frac{foc^2\lambda^2}{\pi^2 D^2} \sum_{j=4}^{\infty} b_j^2, \tag{3}$$

where foc is the focal length of the lens and D is the aperture diameter. Using this relation, model-based algorithms, in which test perturbations are applied by adding basis Lukosz modes to the wavefront, can determine the corresponding Lukosz coefficients of an unknown wavefront. If, while probing a given aberration L_{j0}, the algorithm uses two test perturbations $+\varepsilon_0 L_{j0}$ and $-\varepsilon_0 L_{j0}$, where ε_0 is the test perturbation value (amplitude), then the unknown aberration coefficient b_{j0} is calculated as:

$$b_{j0} = \frac{R_+^2 - R_-^2}{R_+^2 + R_-^2 - 2R_0^2} \frac{\varepsilon_0}{2}, \tag{4}$$

where R_0^2, R_+^2, R_-^2 are the squared rms spot radii for the initial wavefront and after applying the test perturbation

in the positive and negative directions, respectively. If the algorithm uses a single test perturbation $\varepsilon_0 L_{j0}$ to probe a given aberration, after which the spot radius is R, then the unknown aberration coefficient b_{j0} can be found from the formula:

$$b_{j0} = \frac{\pi^2 D^2}{2\lambda^2 foc^2 \varepsilon_0}(R^2 - R_0^2) - \frac{\varepsilon_0}{2}. \quad (5)$$

The difference between the calculations using formulas (4) and (5) is that in the second case the determining expression includes the parameters of the optical system, whereas in the first case it does not. Expression (4) indirectly includes only the radiation wavelength, which is needed to relate the corrector deflection in length units to the wavefront deflection in phase units. The algorithm with two test perturbations makes it possible to exclude the aperture diameter and the focal length of the lens from the calculations. The algorithm with a single test perturbation using formula (5) is preferable for maximum speed of AOS operation in the presence of dynamic aberrations [17,29].

Thus, the property (2) of Lukosz polynomials allows one to use the relation (3) to implement a probing algorithm where aberration coefficients are calculated using formulas (4) and (5). It is clear that relation (3) holds true for all mode bases with property (2), which lets us pass to other bases in these model-based algorithms. Let us write the wavefront (1) in the basis of Karhunen–Loéve–Lukosz functions $\{\Lambda_j\}$ with the corresponding aberration coefficients $\{\beta_j\}$:

$$\Phi = \sum_{j=1}^{\infty} \beta_j \Lambda_j. \quad (6)$$

Then formula (3) remains valid if we replace $b_j \to \beta_j$, and formulas (4) and (5) hold for the Karhunen–Loéve–Lukosz coefficient β_{j0} with the chosen test perturbation amplitude E_0 (if we replace $\varepsilon_0 \to E_0$).

Below using numerical simulation, we compare the performance of model-based algorithms that operate with two control mode bases: Lukosz polynomials L and Karhunen–Loéve–Lukosz functions $LKL(\Lambda)$. Two types of such algorithms are considered: fast algorithms [15–17], which calculate the unknown aberration coefficients using formulas (4) and (5), and the sequential correction algorithm, which does not compute aberration coefficients by any formulas [18] (operating in a single global iteration mode). The latter algorithm also allows these coefficients to be determined with some accuracy (we will refer to this algorithm simply as the „sequential correction algorithm“ (SCA or SEQ.)). Recall that in the current version of the sequential correction algorithm, the test perturbation amplitude ε_0 (or E_0) is halved at each subsequent step. Thus, for a search depth of, say, 3, the determined aberration coefficients can take one of the following values: $\pm\varepsilon_0$, $\pm 1.5\varepsilon_0/0.5\varepsilon_0$, $\pm 1.75\varepsilon_0/1.25\varepsilon_0/0.75\varepsilon_0/0.25\varepsilon_0$, 0.

Note that the fast algorithms will be simulated in so-called „synchronous mode“ with sequential correction too [16,17], when each aberration is corrected immediately after it is measured. In synchronous mode, each aberration term (mode) requires one additional iteration. Therefore, these algorithms can be referred to as „2N“ and „3N“ fast algorithms [29]. This operating mode is more suitable for practical implementation of the algorithms in the presence of dynamic aberrations, which is particularly relevant for Kolmogorov turbulence [17]. Nevertheless, we present simulation results for static phase screens with a Kolmogorov aberration spectrum (as was also done in the first part of [17]). This corresponds to the maximum achievable wavefront correction quality for an ultra-high-speed AOS. The calculations are performed for an ideal wavefront corrector and for real correctors, specifically, the chosen optimized models of stacked-array piezoelectric deformable mirrors [30]. Some mirrors have a sufficiently high spatial resolution, while others have a lower resolution. In contrast to our earlier work [18], which used the geometric optics approximation with a ray spot diagram, the focal spot here is modeled within the wave optics approximation (as also done in [25]). Presented here results include the achievable rms wavefront error and the chosen laser focusing parameters that have been compared to their initial values, and the errors in determining the aberration coefficients.

2. Numerical simulation of the algorithms using Lukosz and Karhunen–Loéve–Lukosz control modes with an ideal corrector

Let us consider the problem of wavefront correction using model-based algorithms. In this section, we assume that the corrector is ideal, i.e., it reproduces the target aberrations exactly without any error and instantaneously, without the transient processes that occur in reality due to oscillations of the mirror's reflecting surface [31]. As in [25], the input data consist of 2000 different wavefront samples whose phase distortion statistics follows the chosen Kolmogorov model, as verified by structure function analysis using a method from [32]). For convenience, we consider wavefronts with the Lukosz tip and tilt modes (modes 2 and 3) subtracted. In theory, this does not affect the correction result, since the algorithms correct modes starting from the second order, and the absence of global tilts does not affect the focal spot structure [26]. Let's choose a turbulence level of $k = D/r_0 = 10$, where D is the diameter of the selected circular aperture and r_0 is the Fried parameter [26]. As the region of interest (ROI) on an intensity sensor, we take a square area in the focal plane with a side length of approximately ~ 400 Airy disk radii. This ensures that the zone containing most of the energy ($> 98\%$, as recommended for practical tasks in [33]) is always included in this area with a large margin. We also make an important remark that has never been mentioned in the literature on this topic: various large regions of interest for focal spot registration can be used in these algorithms due to the fact that the asymptotic intensity distribution in the far field is

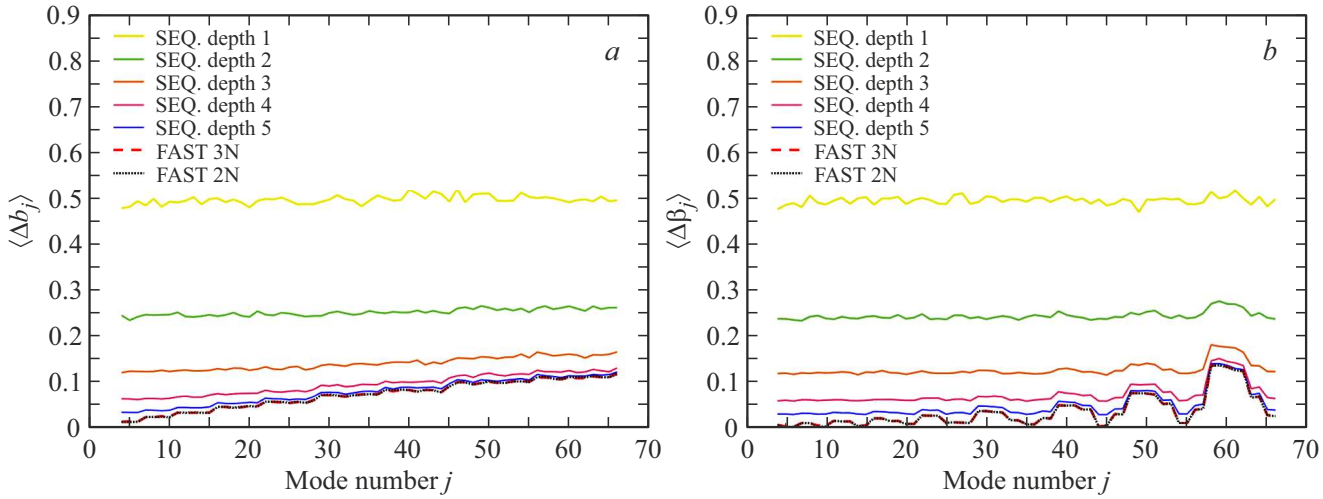

Figure 2. Mean scaled absolute error of aberration coefficient measurement, in units of its mean absolute value, for algorithm operation with an ideal corrector, shown for each mode in the L (a) and LKL (b) bases.

the same regardless of the wavefront shape at the aperture, as one moves radially outward from the optical axis [34]. Thus, enlarging the ROI adds the same constant to the rms focal spot radius, but this constant cancels out when subtraction is performed in formulas (4) and (5). Note that for a large ROI, the change in the optimization criterion R during probe perturbations is very small; therefore, the results obtained correspond to the case of an ideal CCD camera (no noise, very high resolution). We also note that numerical simulation has shown that using a square region rather than a circular one (as is common [12–17,20]) leads to higher accuracy in determining the aberration coefficients.

In model-based algorithms, the test perturbation amplitude is also a parameter that must be chosen appropriately. For fast algorithms, it is clear that the coefficients $\varepsilon_0(E_0)$ should be chosen neither too small nor too large compared to the measured wavefront coefficient b_{j0} (β_{j0}). For Kolmogorov turbulence, the absolute value of each aberration coefficient follows a half-normal distribution, since the coefficient itself is normally distributed: $N(0, \sigma^2)$. In connection with it, for probing each aberration coefficient b_{j0} (β_{j0}), we chose the test perturbation amplitude $\varepsilon_0(E_0)$ to be equal to the median of the distribution $\sigma\sqrt{2}\mathrm{erf}^{-1}(1/2)$, where erf^{-1} is the inverse of the Gaussian error function. This choice corresponds to the statistically minimal difference between the absolute value of the coefficient being determined and the test perturbation amplitude. For the sequential correction algorithm [18], the maximum value of the corrected aberration is twice the initial test perturbation amplitude. Therefore, taking into account the „three-sigma“ rule, this initial value was set to 1.5σ (simulation also showed that this yields a more accurate results than, for example, 1.0σ).

Since the algorithms determine the coefficients of the probed aberrations of a wavefront, it is useful to consider the mean absolute error of each aberration coefficient, expressed in units of the mean value of that coefficient. Relative error is not a suitable metric here, because for small aberration coefficients it can become very large, but this has almost no effect on laser radiation properties. We will also compare the correction results for different algorithm variants using the rms wavefront error criterion and the laser focusing parameters employed in [25]: peak Strehl ratio St, on-axis Strehl ratio $St0$, power in the Airy disk (PIB, power in the bucket [26]), $\bar{\beta}$-factor (number of diffraction radii) [35], and the rms spot radius R.

Fig. 2, *a* and *b* shows the mean absolute error of the aberration coefficient measurement, normalized by the mean absolute value of the coefficient, for each basis mode from 2nd to 10th orders (modes 4–66): (a) for L modes: $\langle|\Delta b_j|\rangle$, and (b) for LKL modes: $\langle|\Delta\beta_j|\rangle$. The results are presented in units of the mean absolute value of the aberration coefficient (equal to $\sigma\sqrt{2/\pi}$ — for the fast model-based algorithms (FAST 3N/2N) and the sequential correction algorithm (SEQ. depth: 1,2,3,4,5) when an ideal corrector is used. For a small search depth, the accuracy of the sequential correction algorithm for L and LKL modes is almost the same, and the coefficient measurement error decreases by a factor of two as the search depth increases. After that, however, diffraction effects in the focal spot reduce the growth of the search efficiency. It can be seen that for both L and LKL modes, the accuracy of aberration coefficient measurement is always higher for the fast algorithms, although as the search depth increases, the sequential correction algorithm approaches the accuracy of the fast algorithms. It may be noted that for L modes, the coefficient measurement error in the fast algorithms increases with each successive aberration order. For LKL modes, the error also tends to increase for higher orders. For all modes up to the 9th order inclusive, the LKL aberration modes are measured more accurately (astigmatisms and ⟨CKO⟩, n-fold aberrations are especially good) than the L modes. Only for a very small number of 10th-order modes

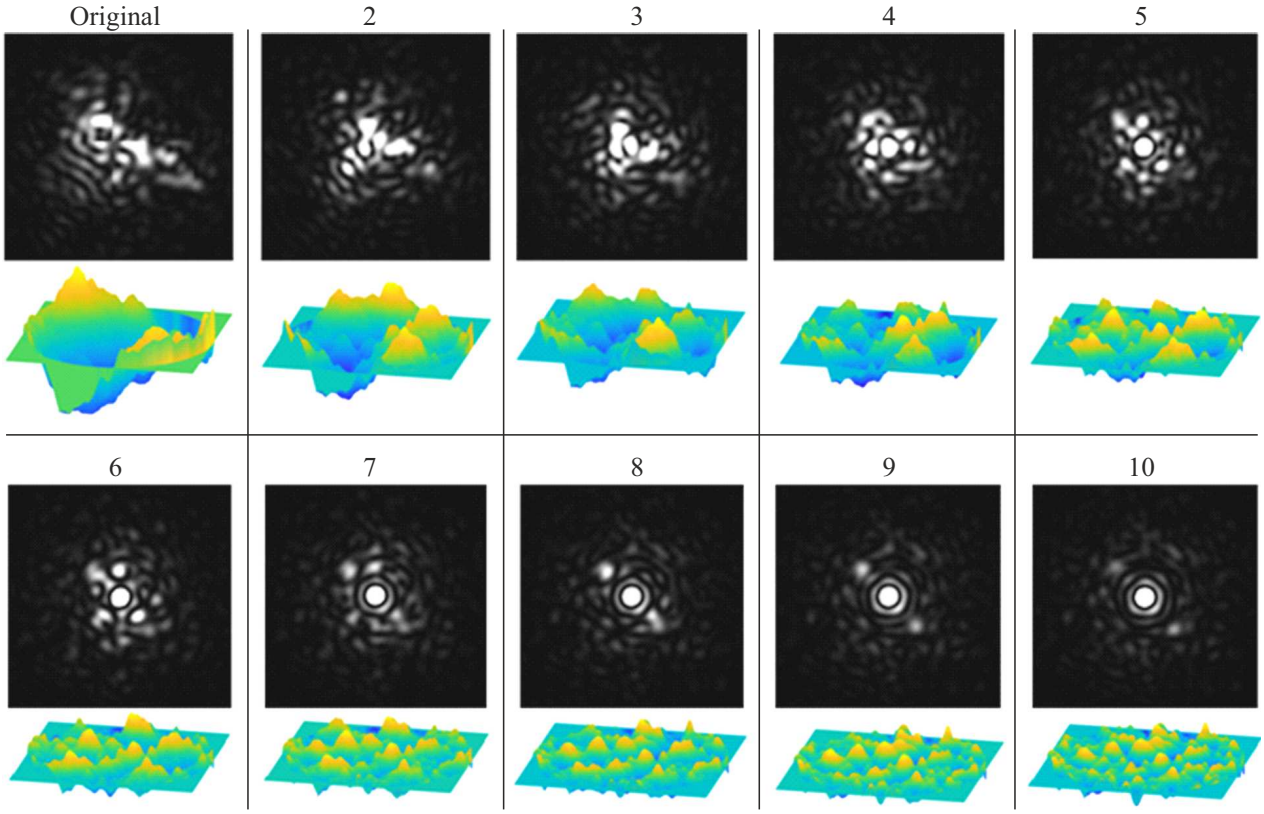

Figure 3. Focal spot appearance and corresponding wavefront profile in the initial state and at each subsequent specified order of modal correction (from 2nd to 10th).

did the measurement error for *LKL* modes turn out to be slightly higher than for *L* modes.

To illustrate how the intensity distribution in the focal spot evolves during wavefront correction, Fig. 3 shows an example of focal spot sequence (high-contrast images) and the corresponding wavefront profiles at successive stages of modal correction (from 2nd to 10th order); i.e., after correcting modes 4–6, 4–10, 4–15, and so on, up to correcting modes 4–66.

Let's take a look on Table 1 that shows mean rms wavefront error and the values of laser focusing parameters achieved by the algorithms considered with an ideal corrector. It can be seen that, depending on the modal correction order, when *LKL* modes are used instead of *L* modes, the rms error of the corrected wavefront decreases by about $\sim 10-40\,\%$, the Strehl ratios increase by $\sim 15-45\,\%$, the power in the Airy disk increases by 15–45%, and the β-factor decreases by about 1%. It is interesting to note that, as also shown in [25], the relative improvement in the focusing parameters for the given turbulence level (10) is greater for modal correction of the 4th order, whereas the relative improvement in the rms wavefront error is greater for modal correction of the 7th and 10th orders. This illustrates the property noted in [25]: the correlation between rms wavefront error reduction and focusing quality improvement is not always strictly direct. As for the difference between the results of the fast algorithms when using an ideal corrector, there is essentially no difference between the 3N and 2N types. Using the sequential correction algorithm (SEQ.) with search depth 5 yields slightly worse laser radiation characteristics. Table 1 shows the equivalents of the English terms used in Fig. 2: SEQ. (sequential correction algorithm), depth, and FAST (fast algorithm).

3. Choosing parameters and actuator layout for deformable mirrors to be used in model-based algorithms

To illustrate a practically relevant case of model-based algorithms operating with real wavefront correctors, we choose appropriate deformable mirror models based on certain target criteria and imposed constraints. We will use stacked-array piezoelectric deformable mirrors in the algorithms — such mirrors are often used for high-power laser radiation propagating through the atmosphere [30,36], as well as in laser-ignited fusion facilities [37]. The actuator influence functions are calculated using the method described in [38]. This allows us to determine how well the basis aberrations can be reproduced by the mirror and subsequently to select optimal actuator layouts and substrate dimensions.

Table 1. Achieved rms wavefront error and laser focusing parameters for the considered model-based algorithms with an ideal corrector

Kolmogorov turbulence level $D/r_0 = 10$		⟨RMS⟩ rad	⟨*St*⟩	⟨*St*0⟩	⟨*PIB*⟩	$\langle\bar{\beta}\rangle$
Initial wavefront		2.59	0.078	0.020	0.067	7.09
Correction of *L* modes with an ideal corrector						
SEQ, depth 5	4th-order modal correction	1.24	0.224	0.222	0.195	6.38
	7th-order modal correction	0.82	0.512	0.512	0.420	5.96
	10th-order modal correction	0.62	0.683	0.682	0.564	5.62
Fast algorithm 3N	4th-order modal correction	1.24	0.225	0.224	0.195	6.38
	7th-order modal correction	0.82	0.515	0.515	0.422	5.96
	10th-order modal correction	0.61	0.687	0.687	0.566	5.62
Fast algorithm 2N	4th-order modal correction	1.24	0.225	0.223	0.195	6.38
	7th-order modal correction	0.82	0.514	0.514	0.421	5.96
	10th-order modal correction	0.61	0.686	0.686	0.565	5.62
Correction of *LKL* modes with an ideal corrector						
SEQ, depth 5	4th-order modal correction	1.10	0.310	0.303	0.280	6.32
	7th-order modal correction	0.71	0.602	0.602	0.519	5.86
	10th-order modal correction	0.54	0.750	0.750	0.639	5.58
Fast algorithm 3N	4th-order modal correction	1.10	0.312	0.305	0.281	6.31
	7th-order modal correction	0.71	0.607	0.607	0.522	5.86
	10th-order modal correction	0.53	0.756	0.756	0.642	5.58
Fast algorithm 2N	4th-order modal correction	1.10	0.312	0.305	0.281	6.31
	7th-order modal correction	0.71	0.607	0.607	0.522	5.86
	10th-order modal correction	0.53	0.756	0.756	0.642	5.58

Let us take a hexagonal actuator layout. It is often used in deformable mirrors (DMs) because it provides a sufficiently high spatial resolution [36] and is convenient for optimization, since it only depends on a single parameter — the distance between adjacent actuators (pitch). We will remove the six outermost corner-actuators (as in [36], for example), because during mirror operation these actuators often produce too small a deflection and cannot provide sufficient dynamic range.

Let the diameter of the mirror's clear aperture be 200 mm, the step of pitch (distance between adjacent actuators) adjustment — 1 mm and the allowed ranges of substrate diameter and thickness — 200−300 mm and 3−5 mm respectively. We consider two actuator layout configurations: with 5 and 6 "rings", corresponding to total actuator counts of 85 and 121, respectively. This choice is motivated by the fact that 121 actuators allow the mirror to reproduce modes up to the 10th order reasonably well, whereas 85 actuators perform poorly for the highest considered orders. This will allow us to see, in comparison, how algorithm performance degrades when the mirror's spatial resolution is limited.

To compare the performance of the algorithms using Lukosz modes and Karhunen–Loéve–Lukosz modes, we choose the actuator layout according to the criterion of more accurate reproduction of these spatial mode forms by the mirror. It is important to emphasize that while low-order modes can be reproduced reasonably well with the chosen number of actuators for a wide range of actuator pitches (the residual "rms surface error" almost always decreases by at least a factor of 10), the reproduction of high-order modes (9th-10th orders) can be critically dependent on the actuator pitch. In the operation of the considered model-based algorithms each separate basic mode is measured and immediately corrected by the mirror. Therefore, if a high-order aberration is measured with a large error, it will be added to the wavefront with a large amplitude at the next iteration, instead of being corrected. For this reason, when optimizing the DM parameters, we chose cases where the 9th- and 10th- order modes were reproduced in the best possible way. The results obtained in the next section confirm that the chosen DM models allow the model-based algorithms to achieve rms wavefront errors and laser focusing parameters close to those obtained with an ideal corrector.

When choosing the actuator layout, it is also very important to take into account the dynamic range of mirror deflection. We assume that, prior to operation, an initial midpoint bias (in terms of control voltages) is applied to the mirror, so that the mirror can then deform equally in both directions. It should be taken into account that the mirror deflection, when matching the wavefront shape, should be two times smaller [39]. We set the maximum turbulence level for Kolmogorov wavefronts to $k_{\max} = 25$, which is often a reasonable limit in theoretical simulations of such algorithms [14,20]). To relate the phase wavefront to the wavefront profile expressed in wavelength units, we choose the laser wavelength to be $\lambda_0 = 1.053\,\mu$. Such a wavelength value is often used, for example, in laser-ignited fusion

facilities [37]. We allocate 15% of the mirror's dynamic range to correct its own initial shape. This value is typical for mirrors of this type [36]. As mirror drives, we take APM-2-7 actuators [40] with updated values of longitudinal stiffness, equal to $K = 30\,\mathrm{N}/\mu\mathrm{m}$ and a maximum internal tensile force equal to $F_0 = 1000\,\mathrm{N}$. We additionally check that when test perturbations are added to the wavefront, the voltages applied to the mirror actuators also remain within acceptable range. Based on the „three-sigma" rule, we have checked that the mirror, at the chosen wavelength, is capable of reproducing each aberration with a coefficient of $3\sigma k_{\max}^{5/6}$. As expected, this condition turned out to be significantly less restrictive than the condition for reproducing the entire Kolmogorov wavefronts.

Finally, the optimization calculations under the constraints imposed let us design four stacked-array piezoelectric DMs: two with 121 actuators and two with 85 actuators. Fig. 4, *a* and *c* shows the optimized mirror models LM-121 and LKLM-121 for more accurate reproduction of Lukosz polynomials and Karhunen–Loéve–Lukosz functions respectively. The LM-121 mirror has a substrate diameter of 270 mm and an actuator pitch of 22 mm. The LKLM-121 mirror has a substrate diameter of 300 mm and an actuator pitch of 18 mm. The two other optimized lower-resolution mirror models — LM-85 and LKLM-85, for reproducing Lukosz polynomials and Karhunen–Loéve–Lukosz functions, respectively — are shown in Fig. 4 (b,d). The LM-85 mirror has a substrate diameter of 240 mm and an actuator pitch of 24 mm. LKLM-85 mirror has a substrate diameter of 300 mm and an actuator pitch of 22 mm. The substrate thickness of all mirrors is taken to be 3 mm to allow for greater possible deflection.

In our subsequent simulations of the algorithms performance with the chosen DMs, as in the case of an ideal corrector, we assume that the mirror reproduces the specified spatial shapes instantaneously, without transient oscillations. If we additionally consider a constraint on the minimum value of the first natural frequency of the mirror substrate, then for the LKLM-121 and LKLM-85 mirror models, one could choose a smaller substrate diameter — for example 240 mm. The spatial resolution would then degrade only slightly ($< 5\%$ for the $\mathrm{rms}_0/\mathrm{rms}$ criterion) since the part of the substrate outside the actuator zone has very little effect on the mirror deflection. In turn, the first natural frequency would increase by more than two times with such a reduction in substrate diameter.

Table 2 gives, for each considered basis mode (using Noll' indexing scheme for *L* [24] and the corresponding indexing scheme for *LKL* [25]), the values of the $\mathrm{rms}_0/\mathrm{rms}$ ratio i.e., how many times the rms error aberration profile decreases when the corresponding modes are reproduced by these mirrors. It can be seen that mirrors with 85 actuators are significantly inferior to those with 121 actuators in terms of spatial resolution, and this should affect the algorithm performance. In general, *L* modes are being reproduced better than *LKL* modes by the mirrors. However, it should be noted that for low-order (2)−(4) aberrations, all mirrors provide nearly ideal reproduction of the aberration shapes for both Lukosz polynomials and Karhunen–Loéve–Lukosz functions. At the same time, it should be emphasized that for higher-order modes — not extremely high, but somewhat in the middle of the target spatial frequency range — it is not uncommon for *LKL* modes to be reproduced better than *L* modes. Therefore, with an equal number of actuators and the same their layout-type, some *LKL* modes may have an advantage in reproduction over *L* modes.

4. Numerical simulation of the algorithms using Lukosz and Karhunen–Loéve–Lukosz control modes with the developed deformable mirrors

This section presents the results of model-based algorithms performance when the correctors are the DM models developed above. Let's emphasize that hysteresis [30,26] is not taken into account in our analysis. In practice, this could correspond to using actuators with feedback, although the accuracy of hysteresis compensation would then be limited.

Fig. 5 (*a, b*) and (*c, d*) shows the results for $\langle \Delta b_j \rangle$ in units of $\langle |b_j| \rangle$ and $\langle \Delta \beta_j \rangle$ in units of $\langle |\beta_j| \rangle$ respectively. For each case, the DM models LM-121 and LM-85 were used with the *L*-mode algorithms, and the models LKLM-121 and LKLM-85 with the *LKL*-mode algorithms. As expected, compared to the case of an ideal corrector, the accuracy of measuring high-order aberration coefficients deteriorated. A clear correlation is seen between the error in reproduction of a basis aberration and the error in measuring its aberration coefficient. Note that when operating with *L* modes, for some components (modes 56−60 for the LM-121 mirror and modes 29, 37−39, 46−49 for the LM-85 mirror), the accuracy of the sequential correction algorithm slightly exceeded that of the fast 2N algorithm, but by no more than $\sim 2\%$. However, the sequential correction algorithm never outperformed the fast 3N algorithm in terms of accuracy. For wavefront correction using *LKL* modes, the fast algorithms have always been more accurate.

Tables 3 and 4 show the mean rms wavefront errors and laser focusing parameters achieved by the algorithms when operating with the chosen DMs. For mirrors with 121 actuators, the final rms wavefront errors, with very rare exceptions, were the same as for the ideal corrector. The focusing parameters also remained nearly identical. For *L* modes, they even improved slightly in some cases. This can be explained by the fact that during correction the mirror introduced small additional high-frequency aberrations into the wavefront, and the resulting small additional local wavefront slopes were oriented in such a way that they provided a better phase alignment of the secondary waves, which enhanced the constructive interference at the center of the focal spot, increasing the Strehl ratio and the power

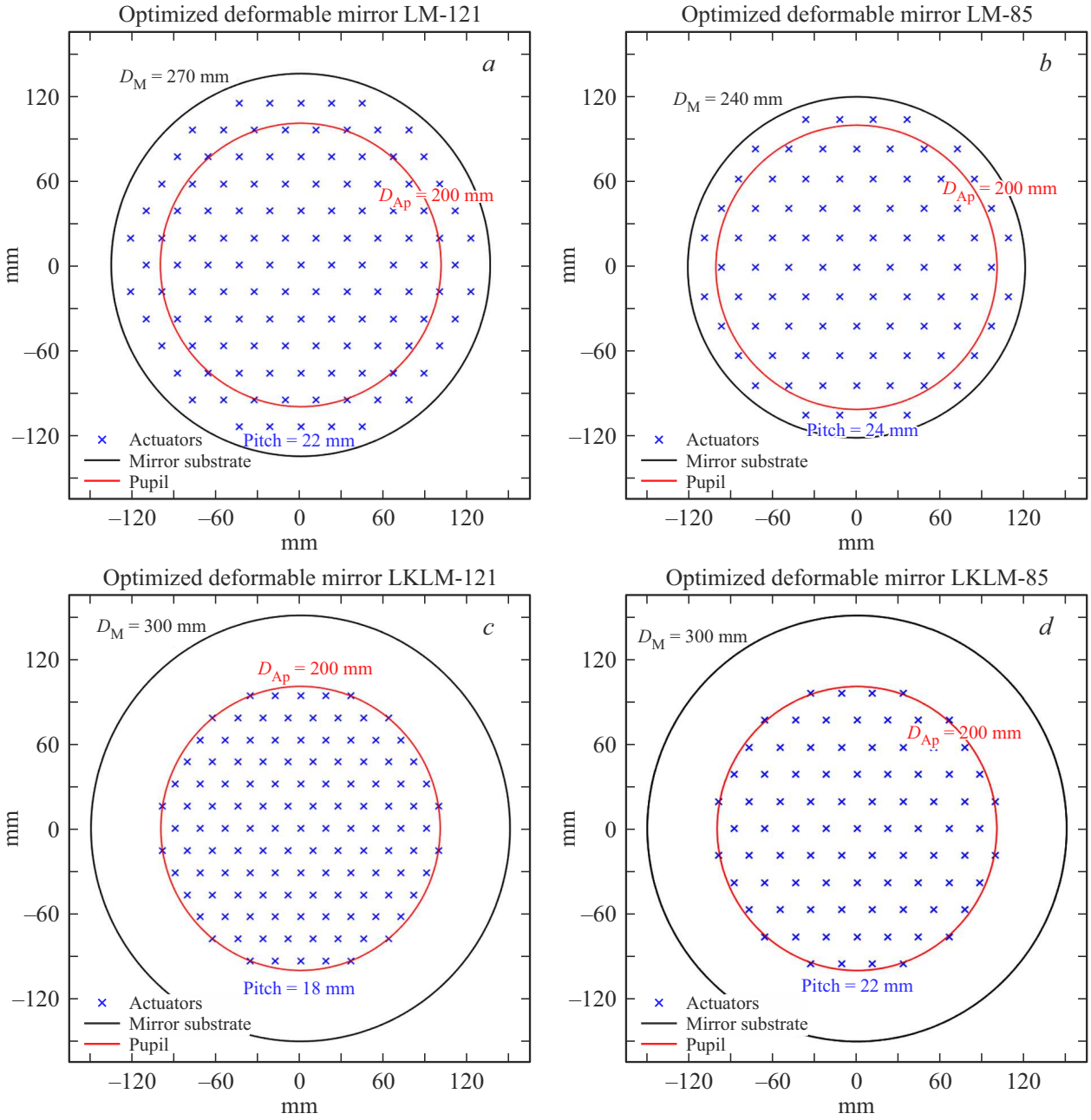

Figure 4. DM models for reproducing *L* and *LKL* modes up to the 10th order inclusive.

in the bucket corresponding to Airy disk. For *LKL* modes, this is not observed, since they already represent shapes with weak high-frequency waviness, which have a more optimal effect on the focusing parameters and should be corrected more accurately without introducing noticeable additional distortions. For mirrors with 85 actuators, the final rms wavefront errors turned out to be slightly larger than in the case of the ideal corrector, but the difference is very small 0.5–3%. The focusing parameters obtained with these mirrors deteriorated by 0.5–2.5% on average. It can be concluded that the characteristics of the LM-85 and LKLM-85 mirrors listed in Table 2 are sufficient for using these DMs to correct Kolmogorov wavefront aberrations of up to the 10th order using the considered model-based algorithms.

Conclusions

In this work, we considered model-based algorithms that operate using the rms spot radius criterion, and for a given statistics of wavefront phase distortions (Kolmogorov spectrum). As control modes, we took the principal components of geometric transverse (ray) aberrations the Karhunen–Loéve–Lukosz functions, which we derived in [25]. It is shown that, statistically, the use of new aberration modes in

Table 2. Accuracy of basis aberration reproduction by the deformable mirrors (left part — when LM-121, LKLM-121 mirrors are in operation; right part — when LM-85, LKLM-85 mirrors are in operation)

№	RMS_0/RMS		№	RMS_0/RMS		№	RMS_0/RMS		№	RMS_0/RMS	
	Modes	Modes		Modes	Modes		Modes	Modes		Modes	Modes
	L	*LKL*		*L*	*LKL*		*L*	*LKL*		*L*	*LKL*
4	15729	832	37	15.1	28.8	4	509	598	37	5.1	11.6
5	27660	333	38	16.1	28.8	5	1640	269	38	5.2	11.6
6	27753	334	39	16.0	19.4	6	1650	270	39	5.1	8.7
7	2997	1922	40	22.1	20.9	7	193	867	40	5.7	8.8
8	2995	1924	41	22.0	21.0	8	193	866	41	5.7	8.8
9	5666	154	42	57.2	25.3	9	370	130	42	6.2	8.8
10	6495	278	43	103	25.3	10	384	177	43	10.2	8.8
11	818	589	44	58.3	23.7	11	56.0	254	44	10.8	9.0
12	992	156	45	58.2	25.7	12	70.3	98.3	45	10.8	9.2
13	987	157	46	8.2	17.4	13	69.8	98.6	46	4.4	6.5
14	2110	140	47	8.2	21.1	14	137	96.6	47	4.4	8.3
15	2100	140	48	9.6	10.6	15	136	96.4	48	4.7	4.5
16	200	187	49	9.3	10.6	16	24.0	107	49	4.0	4.5
17	200	187	50	13.0	10.4	17	24.0	107	50	4.5	4.5
18	445	101	51	13.0	13.3	18	35.4	59.6	51	4.5	4.5
19	424	77	52	15.7	14.5	19	31.2	43.8	52	5.3	4.8
20	913	103	53	15.7	14.5	20	61.5	58.8	53	5.3	4.8
21	915	103	54	35.9	14.7	21	61.4	58.8	54	5.4	5.2
22	78.2	79.4	55	36.7	14.7	22	11.8	41.5	55	11.8	5.2
23	83.2	97.6	56	5.0	12.7	23	12.9	39.0	56	4.9	4.7
24	83.6	97.6	57	5.2	12.7	24	13.0	39.0	57	4.5	4.7
25	217	62.1	58	5.2	5.9	25	18.2	29.8	58	4.5	2.4
26	218	89.6	59	6.2	6.1	26	18.3	40.8	59	3.9	2.5
27	722	62.6	60	6.2	6.1	27	58.2	29.8	60	3.9	2.5
28	390	62.6	61	10.6	6.7	28	24.5	29.8	61	3.5	2.6
29	30.7	37.3	62	7.1	6.7	29	7.1	18.9	62	4.1	2.6
30	30.7	37.2	63	9.6	8.7	30	7.1	18.9	63	4.0	3.3
31	43.2	50.8	64	9.7	8.7	31	7.3	18.4	64	4.0	3.3
32	38.7	44.1	65	24.2	9.1	32	9.4	16.6	65	4.7	3.3
33	118	44.2	66	24.3	9.1	33	11.2	19.5	66	4.7	3.3
34	118	44.2				34	11.2	19.5			
35	102	40.9				35	17.8	16.6			
36	102	40.9				36	17.8	16.6			

the algorithms for modal correction of wavefronts up to the 4th, 7th, and 10th orders (inclusive) at a turbulence level of 10 improves the laser radiation characteristics compared to the classical modes. In particular, depending on the order of modal correction (4, 7, 10), a residual mean rms wavefront error smaller by 10−15% was achieved, and the average laser focusing parameters were improved — the intensity at the focal spot center increased by 10−45%, and the size of the main power concentration (beta-factor) decreased by 1%. The focusing parameters achieved by the algorithms considered are shown in Tables 1, 3, and 4. They differ only by few percent (by 3.3% at most, but typically 1−2%) from those achieved by ideal modal correction, according to our previous work [25]. This also indicates that the choice of DM parameters for the taken actuator layout is close to optimal. This also indicates that the choice of DM parameters for this configuration of mirror drive location is close to optimal.

The mean absolute error of the aberration coefficient measurement, expressed in units of the mean absolute value of the coefficient, is presented. It was found that for almost all modes from the two aberration bases considered Lukosz (*L*) and Karhunen–Loéve–Lukosz (*LKL*) — the coefficients for *LKL* modes are being measured more accurately, both for the ideal corrector and for the chosen deformable mirror models. The difference in accuracy of measurement is typically a few percent, but sometimes reaches 10−30% (the difference is larger for low-resolution mirrors). This

Table 3. Achieved rms wavefront errors and laser focusing parameters for the considered model-based algorithms with the use of LM-121 and LKLM-121 mirrors

Kolmogorov turbulence level $D/r_0 = 10$		⟨RMS⟩ rad	⟨*St*⟩	⟨*St*0⟩	⟨*PIB*⟩	$\langle\bar{\beta}\rangle$
Initial wavefront		2.59	0.078	0.020	0.067	7.09
Correction of *L* modes, mirror LM-121						
SEQ, depth 5	4th-order modal correction	1.24	0.224	0.222	0.195	6.38
	7th-order modal correction	0.82	0.513	0.513	0.421	5.96
	10th-order modal correction	0.61	0.686	0.686	0.569	5.63
Fast algorithm 3N	4th-order modal correction	1.24	0.225	0.224	0.195	6.38
	7th-order modal correction	0.81	0.516	0.516	0.423	5.96
	10th-order modal correction	0.61	0.691	0.691	0.571	5.63
Fast algorithm 2N	4th-order modal correction	1.24	0.225	0.223	0.195	6.38
	7th-order modal correction	0.82	0.514	0.514	0.421	5.96
	10th-order modal correction	0.61	0.685	0.685	0.565	5.63
Correction of *LKL* modes, mirror LKLM-121						
SEQ, depth 5	4th-order modal correction	1.10	0.310	0.303	0.280	6.32
	7th-order modal correction	0.71	0.602	0.601	0.519	5.87
	10th-order modal correction	0.54	0.748	0.748	0.638	5.59
Fast algorithm 3N	4th-order modal correction	1.10	0.311	0.305	0.281	6.32
	7th-order modal correction	0.71	0.606	0.606	0.521	5.87
	10th-order modal correction	0.53	0.755	0.755	0.641	5.59
Fast algorithm 2N	4th-order modal correction	1.10	0.312	0.305	0.281	6.32
	7th-order modal correction	0.71	0.606	0.606	0.521	5.87
	10th-order modal correction	0.53	0.754	0.754	0.641	5.59

Table 4. Achieved rms wavefront errors and laser focusing parameters for the considered model-based algorithms with the use of LM-85 and LKLM-85 mirrors

Kolmogorov turbulence level $D/r_0 = 10$		⟨RMS⟩ rad	⟨*St*⟩	⟨*St*0⟩	⟨*PIB*⟩	$\langle\bar{\beta}\rangle$
Initial wavefront		2.59	0.078	0.020	0.067	7.09
Correction of *L* modes, mirror LM-85						
SEQ, depth 5	4th-order modal correction	1.23	0.227	0.225	0.197	6.38
	7th-order modal correction	0.81	0.520	0.520	0.430	5.95
	10th-order modal correction	0.63	0.673	0.673	0.561	5.67
Fast algorithm 3N	4th-order modal correction	1.23	0.228	0.226	0.198	6.38
	7th-order modal correction	0.81	0.523	0.523	0.431	5.95
	10th-order modal correction	0.63	0.676	0.676	0.562	5.67
Fast algorithm 2N	4th-order modal correction	1.24	0.225	0.223	0.195	6.38
	7th-order modal correction	0.82	0.512	0.512	0.419	5.96
	10th-order modal correction	0.63	0.670	0.670	0.555	5.68
Correction of *LKL* modes, mirror LKLM-85						
SEQ, depth 5	4th-order modal correction	1.10	0.310	0.303	0.280	6.32
	7th-order modal correction	0.72	0.601	0.600	0.518	5.87
	10th-order modal correction	0.55	0.742	0.742	0.632	5.60
Fast algorithm 3N	4th-order modal correction	1.10	0.311	0.305	0.281	6.31
	7th-order modal correction	0.71	0.605	0.605	0.520	5.87
	10th-order modal correction	0.54	0.748	0.748	0.636	5.59
Fast algorithm 2N	4th-order modal correction	1.10	0.311	0.305	0.281	6.31
	7th-order modal correction	0.71	0.605	0.605	0.520	5.87
	10th-order modal correction	0.54	0.748	0.748	0.635	5.59

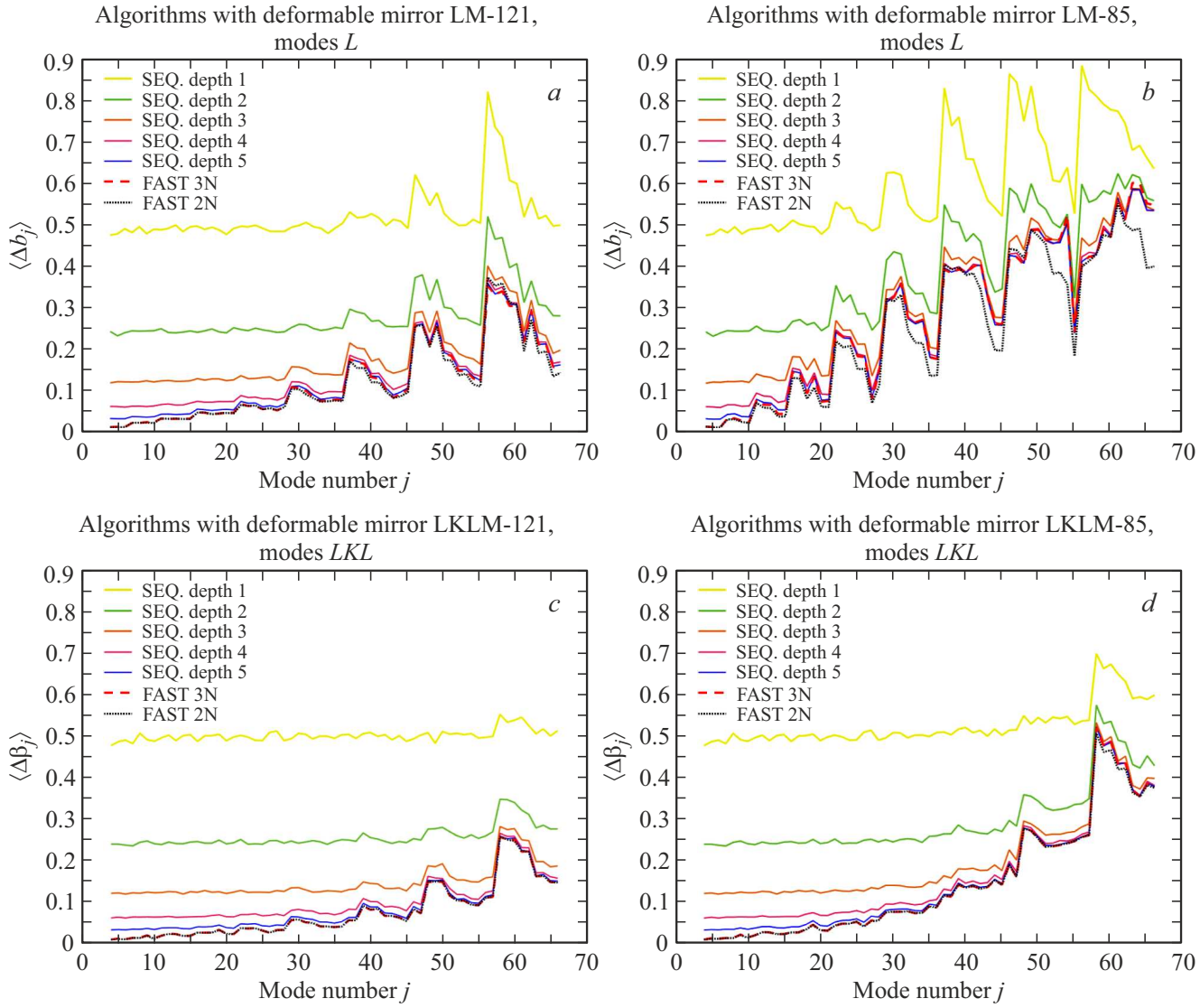

Figure 5. Mean scaled absolute error of aberration coefficient measurement, in units of its mean absolute value, for algorithm operation with the chosen DMs, shown for each of the basis modes: for modes L (a, b), for modes LKL (c, d).

means that the measurement of LKL modes is more robust when the corrector is not ideal. We also recall that in [41] we proposed measuring individual aberration coefficients of atmospheric wavefronts using these model-based algorithms. This approach can be used to determine the dependency on time of the individual wavefront aberration components (as shown in example in [42] on p. 22) in order then to discover their statistical and correlation properties. The results could then be used for predictive adaptive optics algorithms that implement modal correction (including for model-based algorithms [43]).

Let's make an important remark that our reanalysis of the sequential correction algorithm published in [18] has shown that it is less precise than originally claimed almost in all cases, because of diffraction effects unaccounted in [18]. So far we can only conjecture that an optimized scheme of test perturbations in the sequential correction algorithm will improve not only its speed but also its precision, especially with a non-ideal DM.

A comparison of the algorithms using Lukosz modes and Karhunen–Loéve–Lukosz modes shows a twofold advantage of the latter: their correction significantly improves the laser radiation focusing, and the modes themselves (the aberration coefficients) are measured with smaller error. A disadvantage of LKL modes compared to L modes is their higher temporal frequency, which will require high-speed optoelectronic devices in real AOS.

Conflict of interest

The authors declare that they have no conflict of interest.

References

[1] E.A. Vitrichenko. *Adaptivnaya optika. Sbornik statey* (Mir, M., 1980) (in Russian).

[2] M.A. Vorontsov, V.I. Shmalgauzen. *Printsipy adaptivnoy optiki* (Nauka, M., 1985) (in Russian).

[3] L. Ma, B. Wang, Y. Zhou, H. Yang. Proc. SPIE, **10457**, 1045711 (2017). DOI: 10.1117/12.2283378

[4] M.A. Vorontsov, V.P. Sivokon. J. Opt. Soc. Am. A, **15** (10), 2745 (1998). DOI: 10.1364/JOSAA.15.002745

[5] M. Segel, Sz. Gladysz. Opt. Expr., **29** (2), 408682 (2021). DOI: 10.1364/OE.408682

[6] V.A. Bogachev, S.G. Garanin, F.A. Starikov, R.A. Shnyagin. Atm. and Ocean. Opt., **30** (02), 191 (2017). DOI: 10.1134/S1024856017020051

[7] Y. Liu, J. Ma, B. Li, J. Chu. Opt. Engineer., **52** (1), 016601 (2013). DOI: 10.1117/1.OE.52.1.016601

[8] P. Yang, B. Xu, W. Jiang. Front. Optoelectron. China, **1**, 263 (2008). DOI: 10.1007/s12200-008-0068-3

[9] S. Zommer, E.N. Ribak, S.G. Lipson, J. Adler. Opt. Lett., **31** (7), 939 (2006). DOI: 10.1364/OL.31.000939

[10] L. Dong, P. Yang, B. Xu. Appl. Phys. B., **96**, 527 (2009). DOI: 10.1007/s00340-009-3584-y

[11] R. Yazdani, M. Hajimahmoodzadeh, H.R. Fallah. Appl. Opt., **53** (1), 132 (2014). DOI: 10.1364/AO.53.000132

[12] M.J. Booth. Opt. Lett., **32** (1), 5 (2007). DOI: 10.1364/OL.32.000005

[13] H. Linhai, C. Rao. Opt. Expr., **19** (1), 371 (2011). DOI: 10.1364/OE.19.000371

[14] H. Yang, O. Soloviev, M. Verhaegen. Opt. Expr., **23** (19), 24587 (2015). DOI: 10.1364/OE.23.024587

[15] B. Dong, R. Wang. Chin. Opt. Lett., **14** (3), 031406 (2016). DOI: 10.3788/COL201614.031406

[16] W. Lianghua, P. Yang, Y. Kangjian, Ch. Shanqiu, W. Shuai, L. Wenjing, B. Xu. Opt. Expr., **25** (17), 20584 (2017). DOI: 10.1364/OE.25.020584

[17] W. Lianghua, P. Yang, W. Shuai, L. Wenjing, Ch. Shanqiu, B. Xu. Opt. Las. Techn., **99**, 124 (2018). DOI: 10.1016/j.optlastec.2017.08.022

[18] D.A. Yagnyatinskiy, V.N. Fedoseyev. Journ. Opt. Technol., **86** (1), 25 (2019). DOI: 10.1364/JOT.86.000025.

[19] H. Ren, B. Dong. Opt. Expr., **28** (10), 14414 (2020). DOI: 10.1364/OE.387913

[20] H. Yang, Zh. Zhang, J. Wu. Hind. Publ. Corp., 985351 (2015). DOI: 10.1155/2015/985351

[21] T.R. O'Meara. J. Opt. Soc. Am., **67** (3), 318 (1977). DOI: 10.1364/JOSA.67.000318

[22] W. Lukosz. Optica Acta: Int. J. Opt., **10** (1), (1963). DOI: 10.1080/713817744

[23] J. Braat. J. Opt. Soc. Am. A, **4** (4), (1987). DOI: 10.1364/JOSAA.4.000643

[24] V.N. Mahajan. *Optical aberrations and wavefront sensing, part III: Wavefront analysis* (SPIE Press, Bellingham, 2013), p. 388.

[25] D.A. Yagnyatinskiy, A.P. Kuznetsov. Izv. vuzov. Radiofiz., **68** (10), 879 (2025) (in Russian). DOI: 10.52452/00213462_2025_68_10_879

[26] R.K. Tyson. *Principles of adaptive optics* (CRC Press, Boca Raton, 2015).

[27] J.W. Hardy. *Adaptive Optics for astronomical telescopes* (Oxford University Press, N.Y., 1998).

[28] D. Débarre, M.J. Booth, T. Wilson. Opt. Expr., **15** (13), 8176 (2007). DOI: 10.1364/OE.15.008176

[29] H. Ren, B. Dong. Opt. Expr., **29** (17), 27951 (2021). DOI: 10.1364/OE.435171

[30] V.G. Taranenko, O.I. Shanin. *Adaptivnaya optika v priborakh i ustroystvakh* (FGUP „TSNIIATOMINFORM", M., 2005) (in Russian).

[31] L.N. Lavrinova, V.P. Lukin. *Adaptivnaya korrektsiya teplovykh i turbulentnykh iskazheniy lazernogo izlucheniya deformiruemym zerkalom* (Izd-o Inst. opt. atm. SO RAN, Tomsk, 2008) (in Russian).

[32] A.V. Shepelev, D.A. Yagnyatinskiy, V.N. Fedoseyev. Atmos. Ocean. Opt., 37, 476 (2024). DOI: 10.15372/AOO20240408 [A.V. Shepelev, D.A. Yagnyatinskiy, V.N. Fedoseyev. Atmos. Ocean. Opt., **37**, 476 (2024). DOI: 10.1134/S1024856024700647].

[33] D.G. Voelz. *Computational Fourier Optics: A MATLAB Tutorial* (SPIE, Bellingham, 2011).

[34] V.N. Mahajan. *Optical aberrations and wavefront sensing, part II: Wave diffraction optics* (SPIE Press, Bellingham, 2011), p. 45–49.

[35] Ji Zh-Y., Zhang X-F. Proc. SPIE., **10619** (2017). DOI: 10.1117/12.2294622

[36] V. Toporovsky, V. Samarkin, J. Sheldakova, A. Rukosuev, A. Kudryashov. Opt. Las. Techn., **144**, 107427 (2021). DOI: 10.1016/j.optlastec.2021.107427

[37] O.I. Shanin. *Adaptivnye opticheskie sistemy v impusnykh moschnykh lazernykh ustanovkakh* (Tekhnosfera, M., 2012) (in Russian).

[38] D.A. Yagnyatinskiy, V.N. Fedoseyev. Avtom., **57** (1), 68 (2021) (in Russian). DOI: 10.15372/AUT20210108

[39] M. Bass, C. MacDonald, G. Li, C.M. DeCusatis, V.N. Mahajan. *Handbook of optics, V. 5* (OSA, N.Y., 2010).

[40] V.G. Nikiforov. *Mnogosloynye piezokeramicheskie aktyuatory* (OAO „NII Elpa", Zelenograd, 2010) (in Russian).

[41] D.A. Yagnyatinskiy. In: *The XXXI International Symposium „Atmospheric and Ocean Optics. Atmospheric Physics"* (2025). DOI: 10.56820/conferencearticle_6874db6ce743b7.57286392

[42] P. Taghinia. *Wavefront Sensorless Adaptive Optics for Astronomical Applictions*, Thesis (University of Canterbury, Te Whare Wānanga o Waitaha, 2023). URL: https://www.google.com/url?sa=t&source=web&rct=j&opi=89978449&url=https://ir.canterbury.ac.nz/bitstreams/a212bd41-4a31-43ba-8bfe-f7c290ef4bd4/download&ved=2ahUKEwjQi4rM0ZGPAxVeDxAIHVPrCgQQFnoECBcQAQ&usg= AOvVaw3oCwHBsDVVnIPbavA83WmT

[43] P. Piscaer, O. Soloviev, M. Verhaegen. J. Opt. Soc. Am. A., **36** (11), 1810 (2019). DOI: 10.1364/JOSAA.36.001810

Translated by M.Verenikina